

Mössbauer studies of $\text{BaFe}_2(\text{As}_{1-x}\text{P}_x)_2$

K. Komędera¹, J. Gatlik¹, A. Błachowski^{1*}, J. Żukrowski², T. J. Sato³, D. Legut⁴,
and U. D. Wdowik⁵

¹Mössbauer Spectroscopy Laboratory, Institute of Physics, Pedagogical University, Kraków,
Poland

²Academic Center for Materials and Nanotechnology, AGH University of Science and
Technology, Kraków, Poland

³Institute of Multidisciplinary Research for Advanced Materials, Tohoku University, Sendai,
Japan

⁴IT4Innovations Center, VSB-Technical University of Ostrava, Ostrava, Czech Republic

⁵Institut of Technology, Pedagogical University, Kraków, Poland

*Corresponding author: sfblacho@cyf-kr.edu.pl



Keywords:

Fe-based superconductors, spin- and charge-density modulations,
⁵⁷Fe Mössbauer spectroscopy

Abstract

The $\text{BaFe}_2(\text{As}_{1-x}\text{P}_x)_2$ compounds with $x = 0$ (parent), $x = 0.10$ (under-doped), $x = 0.31$, 0.33 , 0.53 (superconductors with $T_c = 27.3$ K, 27.6 K, 13.9 K, respectively) and $x = 0.70$, 0.77 (over-doped) have been investigated by the ⁵⁷Fe Mössbauer spectroscopy versus temperature with special attention paid to regions of the spin density wave, the nematic phase and the superconducting transition. Comparing to the parent compound, the $\text{BaFe}_2(\text{As}_{0.90}\text{P}_{0.10})_2$ exhibits reduced amplitude of SDW and preserved universality class of two-dimensional magnetic planes with one-dimensional spins. The nematic phase region for $x = 0.10$ is characterized by incoherent magnetic order. The $\text{BaFe}_2(\text{As}_{0.69}\text{P}_{0.31})_2$ shows coexistence of weak magnetic order and superconductivity due to vicinity of the quantum critical point. The charge density modulations are perturbed near T_c for $\text{BaFe}_2(\text{As}_{0.67}\text{P}_{0.33})_2$ and $\text{BaFe}_2(\text{As}_{0.47}\text{P}_{0.53})_2$ superconductors. Pronounced hump of the average quadrupole splitting across superconducting transition is observed for $x = 0.33$. The phosphorus substitution increases the Debye temperature of $\text{BaFe}_2(\text{As}_{1-x}\text{P}_x)_2$ compound. Moreover, experimental electron charge densities at the Fe nuclei in this material conclusively show that it should be recognized as a hole-doped system. The measured Mössbauer spectral shift and the spectral area remain unaffected by transition to the superconducting state, which indicate that neither the average electron density at the Fe nuclei nor the dynamical properties of the Fe-sublattice are sensitive to the superconducting transition. Theoretical calculations of the hyperfine parameters determining the patterns of the Mössbauer spectra of $\text{BaFe}_2(\text{As}_{1-x}\text{P}_x)_2$ with $x = 0$, 0.31 , 0.5 , and 1.0 were performed within the framework of the density functional theory. These simulations provide an insight into the changes of the immediate neighborhood experienced by Fe atoms upon the P-for-As substitution as well as enable us to explore the influence of P-doping on the electron density, the electric field gradient, and the hyperfine field at iron nuclei in the $\text{BaFe}_2(\text{As}_{1-x}\text{P}_x)_2$ system.

1. Introduction

The BaFe_2As_2 is a metallic parent compound of the iron-based superconductors belonging to the ‘122’ family. Upon cooling one observes a tetragonal-to-orthorhombic structural transition at 139 K accompanied by development of the antiferromagnetic order of itinerant iron moments. The magnetic order has the spin density wave (SDW) character with the iron moments aligned antiferromagnetically along the orthorhombic a axis [1-3]. The superconductivity can be induced by chemical substitution (doping) or hydrostatic pressure. The $\text{BaFe}_2(\text{As}_{1-x}\text{P}_x)_2$ compounds represent ‘Ba-122’ iron-pnictide superconductors with superconductivity induced by nominally “isovalent” chemical doping of the BaFe_2As_2 parent compound (e.g. the partial substitution of As by P) with the wide superconducting dome within the range $0.2 < x < 0.7$ [4]. The highest critical temperature $T_c = 31$ K appears for $x \approx 0.3$. The P-for-As substitution introduces internal strain or distortion, i.e., chemical pressure, because P anion is smaller than As anion. In general, the Fe-based superconductors show high pressure dependence of the T_c reaching +10 K/GPa for under-doped $\text{BaFe}_2(\text{As}_{0.8}\text{P}_{0.2})_2$ and -3 K/GPa for superconductor with $x = 0.35$ [5, 6]. The phosphorus substitution simultaneously suppresses the orthorhombic distortion and the SDW magnetic order with complete disappearance of both transitions at about $x \approx 0.3$ [7, 8]. The c -axis compression with reduction of the average height of pnictogen anions above the iron plane from $h_{\text{As}} = 1.36$ Å for $x = 0$ to $h_{\text{As/P}} = 1.28$ Å for $x = 0.3$ was found [9]. The same substitution level x for suppression of the static long-range magnetic order and for the emergence of the highest T_c indicates the interplay between magnetism and superconductivity in these compounds. This suggests existence of the quantum critical point (QCP) near $x = 0.3$. It is believed that quantum-critical fluctuations originating from the QCP are closely related to the superconductivity through unconventional pairing mechanism and most microscopic theories for Fe-based superconductors are focused on the role of spin- [10, 11], orbital- [12], or nematic- [13, 14] fluctuations to the electron pairing [15].

It is known that ^{57}Fe Mossbauer spectroscopy is sensitive to the shape and amplitude of the SDW [16, 17]. Hence, it is interesting to investigate the changes of the SDW in the under-doped compounds and explore possible existence of the magnetic order near the optimal-doping. Electronic charge modulations in the iron-based superconductors were observed by ^{57}Fe Mossbauer spectroscopy as the s -electrons charge density wave (CDW) and non- s electron (mainly d -electrons) electric field gradient wave (EFGW) [18, 19]. The CDW is a spatial modulation of the charge (electron) density and it can be approximated by the time independent standing plane wave with the spatial period quite often being incommensurate with the lattice period. The s -electrons of the CDW affect the nuclear states of resonant nuclei leading to the distribution of the isomer shifts. For a similar modulation of the density of electrons with angular momentum greater than zero one expects modulation of the electric field gradient (EFG) apart from the constant EFG term arising from local symmetry lower than cubic or some disorder associated with chemical substitution. These modulations are sensitive to the superconducting transition, i.e. they are perturbed upon transition to the superconducting state and recover upon full development of the superconducting gap. Such effects were observed for $\text{Ba}_{0.6}\text{K}_{0.4}\text{Fe}_2\text{As}_2$ [18] with superconductivity induced by hole-doping (partial substitution of Ba by K) and $\text{SmFeAsO}_{0.91}\text{F}_{0.09}$ [19] with superconductivity induced by electron-doping (partial substitution of O by F). In the close vicinity of T_c the effects of enhancement (suppression) of CDW (EFGW) in $\text{SmFeAsO}_{0.91}\text{F}_{0.09}$ are found reverted in $\text{Ba}_{0.6}\text{K}_{0.4}\text{Fe}_2\text{As}_2$. The differences between $\text{SmFeAsO}_{0.91}\text{F}_{0.09}$ and $\text{Ba}_{0.6}\text{K}_{0.4}\text{Fe}_2\text{As}_2$ follow from a different type of doping (electron and hole) required to realize superconductivity in these compounds. Hence, it is interesting to look for similar effects in compounds with superconductivity induced by the isovalent chemical doping. To investigate the spin- and

charge-modulations, the $\text{BaFe}_2(\text{As}_{1-x}\text{P}_x)_2$ samples with $x = 0.10$ (under-doped), $x = 0.31, 0.33, 0.53$ (superconductors) and $x = 0.70, 0.77$ (over-doped) have been studied as a function of temperature by the ^{57}Fe Mössbauer spectroscopy. Superconducting compound with $x = 0.32$ has been investigated previously by A. Sklyarova *et al.* [20]. Results of our Mössbauer spectroscopy experiments are supported by the *ab initio* calculated hyperfine parameters for the $\text{BaFe}_2(\text{As}_{1-x}\text{P}_x)_2$ systems with $x=0, 0.31, 0.50,$ and 0.1 . These theoretical studies, which are based on state-of-the-art density functional theory (DFT) allowed us to clarify a complexity of the measured spectra and relate it to the changes in the local environments of the resonant ^{57}Fe nuclei originating from nominally isovalent doping.

2. Experimental and data evaluation methods

The single crystals of $\text{BaFe}_2(\text{As}_{1-x}\text{P}_x)_2$ compounds were grown by the flux method using mechanically alloyed precursors, as described in Ref. [21]. The single phase quality of the obtained crystals was checked by the XRD and compositions (substitution level x) were determined by the EDX analysis [21]. The critical temperature T_c of the investigated superconductors was determined from the magnetic susceptibility drop (midpoint), while the SDW magnetic ordering temperature T_{SDW} for the under-doped sample was obtained from the temperature of the inflection point in the resistivity [21].

^{57}Fe Mössbauer spectroscopy measurements were performed in transmission geometry using the RENON MsAa-4 spectrometer operated in the round-corner triangular mode and equipped with the LND Kr-filled proportional detector. The He-Ne laser based Michelson–Morley interferometer was used to calibrate a velocity scale. A commercial $^{57}\text{Co}(\text{Rh})$ source made by RITVERC GmbH and kept at room temperature was applied. The source line width $\Gamma_s = 0.106(5)$ mm/s and the effective source recoilless fraction were derived from the fit of the Mössbauer spectrum of the 10- μm -thick $\alpha\text{-Fe}$ foil. The Mössbauer absorbers were prepared in the powder form using 35 mg of the $\text{BaFe}_2(\text{As}_{1-x}\text{P}_x)_2$ compounds mixed with the B_4C carrier. The absorber thickness (surface density) amounted to 17 mg/cm² of the investigated material. The Janis Research Inc. SVT-400 cryostat was used to maintain temperature of absorbers in the range 4.2 K – 300 K. The geometry, count-rate and single channel analyzer window borders were kept constant during all measurements for individual samples constituting an uninterrupted series with increasing subsequent temperatures within the ranges 4.2–75 K and 80–300 K. Two uninterrupted series for each sample are due to liquid helium and liquid nitrogen used as the cooling media, respectively. Recorded data were processed by means of the MOSGRAF software suite.

A transmission integral approximation has been applied to fit Mössbauer spectra exhibiting magnetic hyperfine interaction. The absorption profile accounted for the SDW spectral component was processed by applying a quasi-continuous distribution of the magnetic hyperfine field B . Assuming collinearity of the Fe magnetic moment and the hyperfine field B , one can describe the amplitude of the SDW along the x direction parallel to the wave vector q as a series of odd harmonics following the shape of SDW according to the equation [16, 22, 23]:

$$B(qx) = \sum_{n=1}^N h_{2n-1} \sin[(2n-1) qx].$$

Here the symbol $B(qx)$ denotes a particular magnetic hyperfine field due to SDW at the phase shift qx , where q is the wave number of the SDW and x is the relative position of the Fe atoms along propagation direction of the stationary SDW. The symbols h_{2n-1} denote the amplitudes of subsequent harmonics. The index N enumerates maximum relevant harmonic. The argument qx satisfies the following condition $0 \leq qx \leq 2\pi$ due to the periodicity of SDW. Further details of the Mössbauer spectra evaluation within SDW model can be found in Ref.

[16]. Because the average amplitude of the SDW described by expression (1) equals zero thus the root-mean-square amplitude of the SDW expressed as $\langle B \rangle = \sqrt{\langle B^2 \rangle} = \sqrt{\frac{1}{2} \sum_{n=1}^N h_{2n-1}^2}$ [23]

was used as the average magnetic hyperfine field of the SDW. Here, the parameter $\langle B \rangle$ is proportional to the value of the electronic magnetic moment per unit volume.

The shapes of Mössbauer spectra without magnetic interaction are influenced by the non-vanishing hyperfine electric quadrupole interaction resulting from both crystallographic structure of $\text{BaFe}_2(\text{As}_{1-x}\text{P}_x)_2$ compounds and distortions of the Fe-As layers caused by inserted P atoms. The non-magnetic spectra were fitted with the average electric quadruple splitting $\langle \Delta \rangle$ resulting from the distribution of the quadrupole-split doublets obtained by the Hesse-Rübartsch method in the Lorentzian approximation [24, 25]. The distribution of quadrupole-split doublets originates from a random substitution of As atoms by P atoms which yields different configurations around the iron atoms and finally leads to a perturbation of the local EFG. The spectral line width Γ within the Hesse-Rübartsch distribution fitting method was kept constant and equal to the natural line width. The average center shifts $\langle \delta \rangle$ of each considered here Mössbauer spectrum is given with respect to the center shift of the room temperature α -Fe.

3. Results and discussion

Representative ^{57}Fe Mössbauer spectra measured at 4.2 K, 80 K and 300 K for the BaFe_2As_2 parent compound and the $\text{BaFe}_2(\text{As}_{1-x}\text{P}_x)_2$ compounds are shown in **Fig. 1**. The room temperature spectra of the parent compound show a single narrow line, whereas the spectra of the substituted samples exhibit asymmetrically broadened pseudo-single line. Both singlet and pseudo-singlets follow from very small electric quadrupole hyperfine interaction, i.e., small EFG at the Fe atoms occupying 4d Wyckoff positions in the tetragonal structure of the $I4/mmm$ space group. One also notes that the principal axis of the EFG tensor lies along the crystallographic c axis. The Mössbauer spectra of the $\text{BaFe}_2(\text{As}_{1-x}\text{P}_x)_2$ compounds are more complex and require fitting with the distribution of quadrupole-split doublets due to doping-induced disorder and perturbation of the Fe-As layers by the P atoms which are almost randomly distributed.

A development of the SDW magnetic order with roughly rectangular shape is seen at 4.2 K for the parent and under-doped compounds. The shape of spin modulation indicates that the SDW order is almost indistinguishable from the simple antiferromagnetic order close to the ground state as long as the Mössbauer spectroscopy is concerned.

The under-doped $\text{BaFe}_2(\text{As}_{0.90}\text{P}_{0.10})_2$ sample presents strongly perturbed SDW magnetic order with $T_{\text{SDW}} = 106$ K determined on the basis of the anomaly in the electrical resistivity [21]. At 4.2 K, the average hyperfine magnetic field of the SDW $\langle B \rangle = 4.11$ T is significantly reduced in comparison with the value of the parent compound BaFe_2As_2 with $\langle B \rangle = 5.28$ T. The measured hyperfine magnetic field can be estimated as $\langle B \rangle = \alpha \mu_{\text{Fe}}$, where μ_{Fe} is the on-site magnetic moment of iron atom and α denotes the constant, which is specific for a given compound [26]. In converting the hyperfine magnetic field to the iron magnetic moment, we used $\alpha = 6.1$ T/ μ_{B} , which results from $\langle B \rangle$ obtained for BaFe_2As_2 [16] and $\mu_{\text{Fe}} = 0.87$ μ_{B} determined from the neutron-diffraction measurements [27]. Hence, the hyperfine magnetic field $\langle B \rangle$ at 4.2 K for under-doped $\text{BaFe}_2(\text{As}_{0.90}\text{P}_{0.10})_2$ corresponds to $\mu_{\text{Fe}} = 0.67$ μ_{B} . Similarly, small values of μ_{Fe} and the corresponding α constants were determined from the neutron diffraction and Mössbauer studies of other '122' parent compounds of the Fe-based superconductors. For example, $\mu_{\text{Fe}} = 0.80$ μ_{B} ($\alpha = 11.2$ T/ μ_{B}) for CaFe_2As_2 [28], $\mu_{\text{Fe}} = 0.94$ μ_{B} ($\alpha = 9.5$ T/ μ_{B}) for SrFe_2As_2 [29], and $\mu_{\text{Fe}} = 0.99$ μ_{B}

($\alpha = 8.1 \text{ T}/\mu_B$) for EuFe_2As_2 [30] have been reported. Different scenarios were suggested to explain small values of the iron magnetic moments. Most likely such small magnetic moments are related to a prominent itinerant character of iron spins.

The hyperfine field $\langle B \rangle$ in $\text{BaFe}_2(\text{As}_{0.90}\text{P}_{0.10})_2$ rapidly decreases for temperature above T_{SDW} , but the residual magnetic order is observed up to 130 K, i.e., about 25 K higher than the coherent SDW order, see **Fig. 2** and **Fig. 3**. It was found [7] that the under-doped $\text{BaFe}_2(\text{As}_{0.90}\text{P}_{0.10})_2$ compound in temperature range between T_{SDW} and 130 K is characterized by electronic anisotropy in the crystallographic a - b plane with broken rotational symmetry, but preserved translational symmetry, called the nematic phase. Hence, the Mössbauer spectroscopy results reveal that the nematic phase seems to be a region of incoherent spin density wavelets typical for a critical region. Temperature evolution of the SDW hyperfine magnetic field $\langle B \rangle(T)$, which is shown for $\text{BaFe}_2(\text{As}_{0.90}\text{P}_{0.10})_2$ in **Fig. 3** was fitted within the model described in Ref. [16]. The static critical exponent of 0.13(1) and the coherent SDW order temperature of 110(1) K were obtained. The value of the critical exponent is the same as in the respective parent compound [3, 16]. Therefore, in spite of substitution the universality class remains (1, 2) and indicates that the electronic spin system with SDW obeys the Ising model (one-dimensional spin space), and it has two dimensions in the configuration space (magnetized planes).

The $\text{BaFe}_2(\text{As}_{0.69}\text{P}_{0.31})_2$ superconductor with $T_c = 27.3 \text{ K}$ shows traces of the magnetic order below 60 K, i.e. also within the superconducting state, see **Fig. 2** and **Fig. 3**. The hyperfine field $\langle B \rangle$ (4.2 K) = 2.20 T corresponds to approximately $0.36 \mu_B$ iron moment. The coexistence of magnetism and superconductivity is probably due to vicinity of the quantum critical point reported for this composition [31]. Despite a small jump of about 0.1 T between 26 K and 28 K, which slightly exceeds the error of the measured values, no change of the average magnetic field $\langle B \rangle$ at the critical temperature is observed. The spectra above 60 K, i.e. at temperatures at which no magnetic dipole hyperfine interaction was detected, are fitted with the distribution of the EFG.

The Mössbauer spectra of $\text{BaFe}_2(\text{As}_{0.67}\text{P}_{0.33})_2$ and $\text{BaFe}_2(\text{As}_{0.47}\text{P}_{0.53})_2$ superconductors with $T_c = 27.6 \text{ K}$ and 13.9 K , respectively, display no magnetic dipole hyperfine interaction and thus they were fitted using the distribution of the EFG in the whole temperature range. The EFG distribution is caused by perturbation of the iron surrounding by the phosphorus atoms in the Fe-As layer. A relatively wide distribution range with the quadrupole splitting Δ reaching up to about 1.6 mm/s (or more) was also observed for others optimally doped Fe-based superconductors [18, 19] and it was interpreted as the presence of the EFG spatial modulation, called the electric field gradient wave (EFGW). Such high splitting Δ could be observed for highly covalent bonds of iron with the electron(s) located in one of the lobes of the 3d ‘atomic’ state. Such electronic configuration is consistent with the observed (and reported in the text below) spectral center shift of about 0.5 mm/s at the ground state. It was found that the average quadrupole splitting $\langle \Delta \rangle$ varies at the critical temperature for $x = 0.33$, i.e. for optimally-doped superconductor with the highest T_c in our studies, see **Fig. 2** and **Fig. 3**. Variation is characterized by an increase of $\langle \Delta \rangle$ at T_c probably due to the opening of the superconducting gap and subsequent formation of the Cooper pairs. The similar effect was observed previously for others Fe-based superconductors [18, 19], for which the perturbation of the spatial modulation of the EFG, being a consequence of the incommensurate modulation of the electron charge density at the Fe nuclei, was found.

Despite some tiny change in the Mössbauer spectra shape near T_c (see **Fig. 3**), no change of the $\langle \Delta \rangle$ at T_c was detected while applying the Hesse-Rübartsch distribution fitting model for $\text{BaFe}_2(\text{As}_{0.47}\text{P}_{0.53})_2$ superconductor. This subtle effect is visible only when the spectral line width Γ of the Hesse-Rübartsch distribution is not a constant value. In such a case, the oscillations of the Γ of about 0.04 mm/s across the T_c can be observed. It is known

that a signature of the CDW can be seen as the excess of the Mössbauer spectral line width [18, 19]. Oscillations of the spectral line width Γ due to sole variation of the isomer shift correspond to the oscillations of the electron density at the Fe nuclei [32] across formation of the superconducting state of about $0.15 \text{ el./}(\text{Bohr radius})^3$. On the other hand, no change in the electron charge density modulations and spectral shapes was observed for the over-doped compounds with $x = 0.70$ and 0.77 in the whole investigated temperature range.

Temperature dependencies of the average center shift $\langle\delta\rangle$, which are given with respect to $\alpha\text{-Fe}$ at room temperature are shown in **Fig. 3**. At 4.2 K, the $\langle\delta\rangle$ changes from 0.55 mm/s for the parent compound to 0.45 mm/s for $x = 0.77$ over-doped compound, whereas at 300 K, the $\langle\delta\rangle$ changes from 0.43 mm/s for the parent compound to 0.33 mm/s for the over-doped one. The value of this hyperfine parameter indicates that Fe atoms are likely in a low-spin Fe(II) electronic configuration. A decrease in $\langle\delta\rangle$ with increasing substitution level x indicates that phosphorus atoms increase the s -electrons charge density at the Fe nuclei in $\text{BaFe}_2(\text{As}_{1-x}\text{P}_x)_2$ due to weakening of the shielding effect caused by the d -electrons. Therefore, the replacement of As by P in the investigated system decreases the conducting d -electrons charge density and can be interpreted as hole-doping. Indeed, for the optimally doped $\text{BaFe}_2(\text{As}_{0.67}\text{P}_{0.33})_2$ superconductor the shift $\langle\delta\rangle$ equals to 0.51 mm/s at 4.2 K and 0.39 mm/s at RT which is almost exactly the same as for the optimally hole-doped $\text{Ba}_{0.6}\text{K}_{0.4}\text{Fe}_2\text{As}_2$ at the same temperatures [18]. Sizable amount of holes in the hole Fermi surfaces induced by P-for-As substitution in $\text{BaFe}_2(\text{As}_{1-x}\text{P}_x)_2$ was also found by the ARPES spectroscopy [6]. On the other hand, the $\langle\delta\rangle$ for optimally electron-doped Ba-122 superconductors such as $\text{Ba}(\text{Fe}_{1-x}\text{T}_x)_2\text{As}_2$ ($T = \text{Co}$ [22, 33], Ni [34], Rh [35]) amounts to 0.55 mm/s at the ground state, which is exactly the same as for BaFe_2As_2 . This result raises the question “to where the injected electrons go?”. Although a possible answer can be found in Ref. [36], one has to note that the substitution level x due to the transition metal T, which is sufficient for optimal doping, remains low and it is usually much smaller than 0.1. The $\text{Ba}(\text{Fe}_{1-x}\text{T}_x)_2\text{As}_2$ system also offers the opportunity for the isovalent doping for $T = \text{Ru}$. In $\text{Ba}(\text{Fe}_{0.5}\text{Ru}_{0.5})_2\text{As}_2$ with $T_c = 20 \text{ K}$, the $\langle\delta\rangle = 0.55 \text{ mm/s}$ at 5 K was found [37]. This suggests that $\text{Ba}(\text{Fe}_{1-x}\text{Ru}_x)_2\text{As}_2$ can be regarded as truly isovalent doped system due to fact that even at high substitution level x the electron density detected by the Mössbauer spectroscopy is exactly the same as in BaFe_2As_2 .

The temperature dependencies of the spectral shift $\langle\delta\rangle$ shown in **Fig. 3** represent only a typical second-order Doppler shift δ_{SOD} variability with temperature (a relativistic effect due to the thermal motion of the absorbing nuclei) and they were treated in terms of the Debye approximation for the lattice vibrations of Fe atoms. Our experimental data show that the Debye temperature Θ_D is typical for the strongly bound metal-covalent system. It increases with phosphorus substitution level from 419(7) K for parent compound, through 456(4) K for superconductor with the highest T_c , to 470(5) K for the over-doped compounds. It means that the Fe–As/P bonds become stiffer with increasing P content. The present experimental data evaluated with the quadrupole distribution and without magnetic interaction indicate that the spectral shifts $\langle\delta\rangle$ for the doping levels $x = 0.31$ (for clarity not shown in **Fig. 3**) and $x = 0.33$ almost overlap between 80 and 300 K. They are, however, not in accordance with the experimental data from the low temperature range, i.e. where contribution of magnetic interactions becomes significant and makes the spectra extremely complex. Thus, the resulting $\Theta_D = 464(7) \text{ K}$ for $x = 0.31$ was estimated using the data from “high” temperature.

The $\Theta_D = 459(4) \text{ K}$ for $\text{Ba}_{0.6}\text{K}_{0.4}\text{Fe}_2\text{As}_2$ superconductor (see **Fig. 4**) was calculated for comparison from the $\delta(T)$ dependence based on partly unpublished data, that were obtained during measurements reported in Ref. [18]. Similar value of the Debye temperature for both optimally-doped superconductors ($\text{BaFe}_2(\text{As}_{0.67}\text{P}_{0.33})_2$ and $\text{Ba}_{0.6}\text{K}_{0.4}\text{Fe}_2\text{As}_2$) is a strong indication that iron dynamics is the same in both compounds as it depends on the “inner”

dynamics of nearly the same Fe–As/P (pnictogens) sheets. On the other hand, the values of the Θ_D found here are much larger than the reported $\Theta_D = 250$ K for BaFe_2As_2 , which has been derived from the specific heat measurements [38]. The most probable reason for this discrepancy is a different weight of the phonon frequency distribution used in determination of the Θ_D from the specific heat data as compared to that gained from the Mössbauer spectroscopy parameters.

The Mössbauer spectroscopy recoilless fraction f expressed by the Lamb–Mössbauer factor (the analog of the Debye–Waller factor in the coherent neutron and X-ray scattering) is another parameter sensitive to the lattice dynamics. However, due to multitude of the hyperfine interactions affecting the shape of the measured $\text{BaFe}_2(\text{As}_{1-x}\text{P}_x)_2$ spectra, a simplified parameter proportional to the f , called the *RSA*, was used.

The relative spectral area (*RSA*) plotted versus temperature in **Fig. 5** is defined as:

$$RSA = \left(\frac{1}{C} \right) \sum_{n=1}^C \frac{N_0 - N_n}{N_0},$$

where C denotes the number of data channels for the folded spectrum, N_0 is the average number of counts per channel far-off the resonance (i.e. the baseline), and N_n stands for the number of counts in the channel n . Thus, the *RSA* is calculated based only on the original data from measurements and the simple expression defining parameter *RSA* does not depend on any physical model. It should be emphasized that all Mössbauer spectra belonging to the respective set of *RSA* shown in **Fig. 5** were recorded during an uninterrupted series with increasing subsequent temperatures, with the same source kept under the same conditions, within the same geometry, with the same velocity scale and the number of data channels, with the same background under the resonant line and within the linear response range of the detector system. A slight increase of the *RSA* at 130 K for $x = 0.10$ is seen and it could be explained as the increase of the average recoilless fraction due to the magneto-elastic effect. Hence, one can conclude that lattice somewhat hardens upon incoherent magnetic ordering (the nematic phase in this case), and this feature seems to be common to the iron–pnictogen bonds [39, 40]. On the other hand, the *RSA* for $x = 0.31, 0.33$ and 0.53 across superconducting transition is flat and without any irregularity. So, spectral parameters dependent on the lattice dynamics, e.g. recoilless fraction (approximated by the *RSA*) and second-order Doppler shift (included in $\langle \delta \rangle$) are insensitive to the transition. Hence, the lattice dynamics seems unaffected by a transition to the superconducting state.

4. Calculations of the Mössbauer hyperfine parameters by the DFT methods

In order to qualitatively describe modifications of the hyperfine parameters resulting from the substitution of the As atoms by P ones in $\text{BaFe}_2(\text{As}_{1-x}\text{P}_x)_2$ system, we resort in the following to parameter-free first-principles calculations realized by DFT method. In particular we examine the electron density (isomer shift), the electric field gradient (quadrupole splitting), and the hyperfine magnetic field.

The $\text{BaFe}_2(\text{As}_{1-x}\text{P}_x)_2$ compositions at $x = 0.0, 0.31, 0.5, 1.0$ were modeled by the $1 \times 1 \times 1$ ($x = 0.0, 0.5, 1.0$) and $2 \times 2 \times 1$ ($x = 0.31$) supercells obtained from the ideal BaFe_2As_2 structure of $I4/mmm$ (No. 139) space group, in which Ba atoms occupy $2a(0,0,0)$ positions, Fe atoms are located at $4d(0, \frac{1}{2}, \frac{1}{4})$ positions, and As/P atoms reside at $4e(0,0,z)$ sites. To investigate the effect of local environment on the hyperfine parameters at the Fe nuclei due to substitution of As atoms with P atoms, various configurations including four As atoms (4As), three As and one P atoms (3As1P), two As and two P atoms (2As2P), one As and three P atoms (1As3P), and four P atoms (4P) as the nearest-neighbors of Fe atoms have been simulated. Insets in the **Fig. 6** show examples of the modeled $\text{BaFe}_2(\text{As}_{1-x}\text{P}_x)_2$ compositions at

$x = 0.31$ and $x = 0.5$.

Calculations have been performed within the spin-polarized density functional theory (DFT) method using the plane-wave basis VASP code [41] and the full-potential (linearized) augmented plane-wave plus local orbitals [FP-(L)APW + lo] method, the latter implemented in the WIEN2K code [42]. The pseudopotential plane-wave method has been applied to optimize the structures, while the all-electron method has been applied to calculate the hyperfine interactions at the Fe nuclei.

4.1 Calculations with the pseudopotential method

Electron-ion interactions were described by the projector augmented wave (PAW) method [43]. The PAW pseudopotentials with reference configurations for valence electrons Ba($5s^2 5p^6 6s^2$), Fe($3d^7 4s^1$), As($4s^2 4p^3$), and P($3s^2 3p^3$) were taken from VASP database. The gradient-corrected exchange-correlation functional with parametrization of Perdew, Burke and Ernzerhof (GGA-PBE) revised for solid systems (PBEsol) [44] together with a plane-wave expansion up to 400 eV were applied. Spin-polarized calculations with the type-I antiferromagnetic order (AF-I), in which the magnetic moments on the Fe atoms are aligned within the (100) layer and opposite to the moments of the next (100) layer, resulted in the magnetic moments on Fe atoms less than $0.04 \mu_B$. The Brillouin zones of $\text{BaFe}_2(\text{As}_{1-x}\text{P}_x)_2$ structures were sampled with the Monkhorst-Pack k -point meshes of $12 \times 12 \times 4$ ($x = 0.0, 0.5, 1.0$) and $6 \times 6 \times 4$ ($x = 0.31$). The ideal structures with $x = 0.0$ and $x = 1.0$ were fully optimized. Resulting lattice constants and internal atomic coordinates for BaFe_2As_2 ($a = 3.8845 \text{ \AA}$, $c = 12.4580 \text{ \AA}$, $z = 0.3471$) and BaFe_2P_2 ($a = 3.7623 \text{ \AA}$, $c = 12.2530 \text{ \AA}$, $z = 0.3395$) remain in close correspondence to those reported previously [1, 45]. Structural relaxations of $\text{BaFe}_2(\text{As}_{1-x}\text{P}_x)_2$ systems with $x = 0.31$ and $x = 0.5$ were performed for fixed volumes of the supercells followed from the optimized value of the BaFe_2As_2 lattice. Convergence criteria for the residual forces and total energies of 0.01 eV/\AA and 0.01 meV were applied.

4.2 Calculations with the full-potential method

The scalar-relativistic FP-(L)APW method was applied. The wave functions have been expanded into spherical harmonics inside the nonoverlapping atomic spheres having the radii R_{MT} and in the plane waves within the interstitial region. The R_{MT} were set to 2.5, 2.2, 2.0, 1.85 a.u. for Ba, Fe, As, and P, respectively. The maximum l value for the expansion of the wave functions into the spherical harmonics inside the R_{MT} spheres was set to $l_{\text{max}} = 10$, while for the expansion of the wave functions within the interstitial region, the plane-wave cutoff parameter $K_{\text{max}} = 7/R_{\text{MT}}^{\text{min}}$ was applied. The charge density was Fourier-expanded up to $G_{\text{max}} = 12 \text{ Ry}^{1/2}$. States lying more than 8 Ry below Fermi level were treated as the core states. Alike in calculations with the pseudopotential method, the AF-I magnetic arrangement was taken into account and the correlation and exchange potentials were treated within the GGA-PBEsol approximation. Calculations have been carried out for the supercell volumes adopted from the pseudopotential method calculations. Only the atomic positions were relaxed within the FP-LAPW methodology with the force convergence of 0.01 mRy/a.u. . The Brillouin zone integrations were performed with similar Monkhorst-Pack k -point meshes as those used in pseudopotential calculations. All self-consistent calculations have been performed with the energy and charge convergence criteria better than 10^{-6} Ry . The isomer shift has been obtained from the calculated electron contact densities at the resonant nucleus ρ in a given matrix and reference material ρ_0 as $\delta = \alpha(\rho - \rho_0)$, where α stands for the calibration constant characteristic for a particular nuclear transition. Our calculations are performed for the 14.41-keV transition in ^{57}Fe , and the isomer shifts are given with respect to metallic bcc α -Fe upon applying

previously determined $\alpha = 0.291$ (a.u.)³·mm/s [32]. The iron nucleus has been approximated by the homogeneously charged sphere with radius $R_0 = 4.897$ fm. Further technical details of such calculations can be found in our earlier papers [46].

4.3 Results of calculations

Substitution of As atoms with P atoms results in slight local distortions of the FeT_4 (T = As, P) tetrahedra associated with small (0.01 – 0.02 Å) modifications of the interatomic distances between Fe atoms and the surrounding As/P atoms as compared to the respective Fe-As (2.29 Å) and Fe-P (2.18 Å) distances in the ideal BaFe_2As_2 and BaFe_2P_2 compounds. Also the valence charges of ions forming Fe_2T_2 (T = As, P) layers in $\text{BaFe}_2(\text{As}_{1-x}\text{P}_x)_2$ compositions undergo changes, as indicated by the electron topological analysis [47]. Ideal compositions ($x = 0.0, 1.0$) are characterized by the following effective valencies: $\text{Ba}^{1.20+}\text{Fe}_2^{0.11+}\text{As}_2^{0.71-}$, and $\text{Ba}^{1.20+}\text{Fe}_2^{0.15+}\text{P}_2^{0.75-}$. We note evident departure of Fe and T (T = As, P) valences from their formal values (Fe^{2+} , T^{2-}) due to the covalent bonding within the Fe_2T_2 (T = As, P) layers. Effective charges of Fe ions in $\text{BaFe}_2(\text{As}_{1-x}\text{P}_x)_2$ at $x = 0.31$ and $x = 0.5$ are collected in **Table 1**. One observes an increase in the effective valence charge of Fe with increased number of P atoms in its neighborhood. In the limiting cases (4As and 4P configurations) the effective valences of Fe correspond to those in the ideal BaFe_2As_2 and BaFe_2P_2 systems.

Table 1. Effective valence charges of Fe ions in $\text{BaFe}_2(\text{As}_{1-x}\text{P}_x)_2$ with $x = 0.31$ and $x = 0.5$ determined from the electron topological analysis [47]. Values are averaged over all considered configurations.

Substitution x	Effective valence charges (in e) for respective configuration				
	4As	3As1P	2As2P	1As3P	4P
0.31	0.11+	0.12+	0.14+	0.15+	0.16+
0.50	0.11+	-	0.14+	-	-

The changes in local environment of Fe which arise from appearance of substitutional P ions in its closest surrounding are also reflected by the calculated isomer shifts, which decrease with increased number of incorporated P atoms and increased valency of Fe. The range of changes in the calculated isomer shifts for 4As, 3As1P, 2As2P, 1As3P, and 4P configurations in $\text{BaFe}_2(\text{As}_{1-x}\text{P}_x)_2$ at $x = 0.0, 0.31, 0.50, 1.0$ are given in **Table 2**. The calculated chemical isomer shifts IS does not include contribution from the second-order Doppler effect (δ_{SOD}), which is of the order of -0.1 mm/s [32]. The average shift $\langle \text{IS} \rangle$ for $x = 0.31$ is somewhat larger than that for $x = 0.5$ due to increase in the s -electrons charge density with increased level of the P-for-As substitution.

Table 2. The calculated isomer shifts of Fe residing in the 4As, 3As1P, 2As2P, 1As3P, and 4P environments in $\text{BaFe}_2(\text{As}_{1-x}\text{P}_x)_2$ with $x = 0.0, 0.31, 0.5, 1.0$. Isomer shifts are given versus bcc α -Fe. Values are averaged over all configurations considered.

Substitution x	Isomer shift (mm/s) for respective configuration				
	4As	3As1P	2As2P	1As3P	4P
0.0	0.373	-	-	-	-
0.31	0.354-0.361	0.330-0.340	0.304-0.326	0.284-0.298	0.261-0.275
0.50	0.371	-	0.322-0.324	-	0.275
1.0	-	-	-	-	0.202

In general, the quadrupole splittings in $\text{BaFe}_2(\text{As}_{1-x}\text{P}_x)_2$ with $x = 0.31$ show quite a broad distribution spanning the range between 0.14 and 0.58 mm/s. One can, however, distinguish two sub-ranges covering values 0.14 – 0.32 mm/s and 0.34 – 0.58 mm/s. The former one corresponds to 4As and 4P configurations, whereas the latter one is due to the 3As1P, 2As2P, and 1As3P surroundings. In composition with $x = 0.50$, the Fe atoms in 4As and 4P environments exhibit quadrupole splittings of about 0.46 mm/s and 0 mm/s, respectively, while the 2As2P configuration is characterized by the quadrupole splitting of about 0.32 mm/s. The average quadrupole splitting $\langle\Delta\rangle$ has a significantly higher value for $x = 0.31$ than for $x = 0.5$ which remains in perfect agreement with the experimental data. The calculated average hyperfine magnetic field in $\text{BaFe}_2(\text{As}_{1-x}\text{P}_x)_2$ with $x = 0.31$ equals about 3.2 T as compared to that extracted from the spectrum measured for sample having the same composition (2.2 T). According to the experimentally determined phase diagram of $\text{BaFe}_2(\text{As}_{1-x}\text{P}_x)_2$, the composition with $x = 0.5$ is still superconducting and shows no magnetic interactions, as confirmed by the present experimental studies (no magnetic field at the Fe nuclei) as well as theoretical calculations ($\langle B \rangle$ less than 0.1 T).

The DFT calculated hyperfine parameters could be applied to simulate the Mössbauer spectra for substitution levels $x = 0.31$ (optimally doped $\text{BaFe}_2(\text{As}_{1-x}\text{P}_x)_2$ superconductor) and $x = 0.5$. Theoretical spectra are shown in **Fig. 6**. They correlate relatively well with the low-temperature experimental spectra of $x = 0.31$, 0.33, and 0.53 compositions, presented in **Figs. 1 and 2**, which do not display magnetic interactions or those with average magnetic field less than 2 T.

5. Conclusions

It is known that the Mössbauer spectroscopy is sensitive to the spin- and charge-distribution around the resonant nucleus via the magnetic dipole, the electric quadrupole, and monopole interactions. On the other hand, the superconductivity modifies density of the electronic states at the Fermi surface and should have some influence on hyperfine interactions. Comparing to the parent compound, the under-doped $\text{BaFe}_2(\text{As}_{0.90}\text{P}_{0.10})_2$ exhibits reduced amplitude of SDW, but with preserved universality class of well separated two-dimensional magnetic planes with one-dimensional spins. The nematic phase temperature region for $x = 0.10$ is characterized by incoherent spin density order. The $\text{BaFe}_2(\text{As}_{0.69}\text{P}_{0.31})_2$ shows some coexistence of weak magnetic order and superconductivity probably due to vicinity of the quantum critical point.

It has been found previously that ^{57}Fe Mössbauer spectroscopy is sensitive to the superconducting transition in the Fe-based superconductors via change of the electron charge density modulations. The incommensurate with the lattice period charge modulations CDW and EFGW are seen via dispersion of the isomer shift and via distribution of the electric field gradient. The present studies demonstrate that the average EFG and/or the charge density modulations are somewhat perturbed near T_c for $\text{BaFe}_2(\text{As}_{0.67}\text{P}_{0.33})_2$ and $\text{BaFe}_2(\text{As}_{0.47}\text{P}_{0.53})_2$ superconductors. This phenomenon is, however, not so spectacular like in $\text{Ba}_{0.6}\text{K}_{0.4}\text{Fe}_2\text{As}_2$ and $\text{SmFeAsO}_{0.91}\text{F}_{0.09}$. A complexity of the Mössbauer spectra caused by P atoms meddles in the Fe-As layers responsible for superconductivity. Especially for $x = 0.33$ with the optimal doping and the highest T_c pronounced hump of the $\langle\Delta\rangle$ across superconducting transition is seen with partial recovery at the lower temperature once the gap is fully developed and the Bose condensate is separated from the remainder of the electronic system. Anomaly of $\langle\Delta\rangle$ reaches 0.02 mm/s (difference between 12 K and 28 K for $x = 0.33$) and it can be converted into the change of the EFG of about 10^{20} V/m² at the T_c . So, it seems that a distribution of the electrons responsible for the covalent Fe-As/P bonds is somewhat perturbed by the itinerant electrons forming Cooper pairs in this metallic system. Increase of the $\langle\Delta\rangle$ at T_c for $x = 0.33$

is somewhat similar to an increase in the EFGW amplitude at T_c for electron-doped $\text{SmFeAsO}_{0.91}\text{F}_{0.09}$ and it has opposite behavior to the change of EFGW amplitude at T_c for hole-doped $\text{Ba}_{0.6}\text{K}_{0.4}\text{Fe}_2\text{As}_2$.

The phosphorus substitution increases the Debye temperature due to lattice hardening and the $\text{BaFe}_2(\text{As}_{1-x}\text{P}_x)_2$ should be recognized as hole-doped system while considering the change of electron density at the Fe nuclei. The spectral shift $\langle\delta\rangle$, which includes temperature dependent second-order Doppler shift δ_{SOD} , and the spectral area RSA seem not affected by the transition to the superconducting state. This indicates that neither the average electron density at the Fe nuclei nor lattice dynamic properties of the Fe atoms are sensitive to the superconducting transition.

A complexity of the experimental Mössbauer spectra could be to some extent resolved by calculating from first-principles parameters of the electric monopole, electric quadrupole, and magnetic dipole interactions, which determine the measured spectral patterns. Modifications of such parameters as isomer shift, quadrupole splitting, and hyperfine field at the resonant iron nuclei reflect changes in their immediate surrounding originating from the incorporation of P atoms into the As-sublattice.

Acknowledgments

This work was supported by the National Science Centre of Poland under the grant 2018/29/N/ST3/00705.

The DFT Group (DL and UDW) acknowledges the European Regional Development Fund in the IT4Innovations national supercomputing center - path to exascale project No. CZ.02.1.01/0.0/0.0/16_013/0001791 within the Operational Programme Research, Development and Education Czech Science Foundations and the Interdisciplinary Center for Mathematical and Computational Modeling (ICM), Grants No. GA73-17 and No. GB70-12 Warsaw University.

All authors dedicate this article to the memory of Professor Krzysztof Piotr Ruebenbauer.

References

- [1] M. Rotter, M. Tegel, D. Johrendt, I. Schellenberg, W. Hermes, and R. Pöttgen, *Phys. Rev. B* **78**, 020503(R) (2008).
- [2] Y. Su, P. Link, A. Schneidewind, Th. Wolf, P. Adelman, Y. Xiao, M. Meven, R. Mittal, M. Rotter, D. Johrendt, Th. Brueckel, and M. Loewenhaupt, *Phys. Rev. B* **79**, 064504 (2009).
- [3] K. Matan, R. Morinaga, K. Iida, and T. J. Sato, *Phys. Rev. B* **79**, 054526 (2009).
- [4] S. Jiang, H. Xing, G. Xuan, C. Wang, Z. Ren, C. Feng, J. Dai, Z. Xu, and G. Cao, *J. Phys.: Condens. Matter* **21**, 382203 (2009).
- [5] L. E. Klintberg, S. K. Goh, S. Kasahara, Y. Nakai, K. Ishida, M. Sutherland, T. Shibauchi, Y. Matsuda, and T. Terashima, *J. Phys. Soc. Jpn.* **79**, 123706 (2010).
- [6] Z. R. Ye, Y. Zhang, F. Chen, M. Xu, Q. Q. Ge, J. Jiang, B. P. Xie, and D. L. Feng, *Phys. Rev. B* **86**, 035136 (2012).
- [7] S. Kasahara, H. J. Shi, K. Hashimoto, S. Tonegawa, Y. Mizukami, T. Shibauchi, K. Sugimoto, T. Fukuda, T. Terashima, A. H. Nevidomskyy, and Y. Matsuda, *Nature* **486**, 382 (2012).
- [8] D. Hu, Z. Yin, W. Zhang, R. A. Ewings, K. Ikeuchi, M. Nakamura, B. Roessli, Y. Wei, L. Zhao, G. Chen, S. Li, H. Luo, K. Haule, G. Kotliar, and P. Dai, *Phys. Rev. B* **94**, 094504 (2016).

- [9] J. M. Allred, K.M. Taddei, D. E. Bugaris, S. Avci, D. Y. Chung, H. Claus, C. de la Cruz, M. G. Kanatzidis, S. Rosenkranz, R. Osborn, and O. Chmaissem, *Phys. Rev. B* **90**, 104513 (2014).
- [10] D. J. Scalapino, *Rev. Mod. Phys.* **84**, 1383 (2012).
- [11] Q. Si, R. Yu, and E. Abrahams, *Nat. Rev. Mater.* **1**, 16017 (2016).
- [12] H. Kontani and S. Onari, *Phys. Rev. Lett.* **104**, 157001 (2010).
- [13] R. M. Fernandes, A. V. Chubukov, and J. Schmalian, *Nat. Phys.* **10**, 97 (2014).
- [14] H.-H. Kuo, J.-H. Chu, J. C. Palmstrom, S. A. Kivelson, and I. R. Fisher, *Science* **352**, 958 (2016).
- [15] D. Hu, W. Zhang, Y. Wei, B. Roessli, M. Skoulatos, L. P. Regnault, G. Chen, Y. Song, H. Luo, S. Li, and P. Dai, *Phys. Rev. B* **96**, 180503(R) (2017).
- [16] A. Błachowski, K. Ruebenbauer, J. Żukrowski, K. Rogacki, Z. Bukowski, and J. Karpinski, *Phys. Rev. B* **83**, 134410 (2011).
- [17] K. Komędera, A. Pierzga, A. Błachowski, K. Ruebenbauer, A. Budziak, S. Katrych, and J. Karpinski, *J. Alloys Compd.* **717**, 350 (2017).
- [18] A. K. Jasek, K. Komędera, A. Błachowski, K. Ruebenbauer, Z. Bukowski, J. G. Storey, and J. Karpinski, *J. Alloys Compd.* **609**, 150 (2014).
- [19] A. K. Jasek, K. Komędera, A. Błachowski, K. Ruebenbauer, H. Lochmajer, N. D. Zhigadlo, and K. Rogacki, *J. Alloys Compd.* **658**, 520 (2016).
- [20] A. Sklyarova, G. C. Tewari, J. Lindén, O. Mustonen, E.-L. Rautama, and M. Karppinen, *J. Magn. Magn. Matter.* **378**, 327 (2015).
- [21] K. Z. Takahashi, D. Okuyama, and T. J. Sato, *J. Cryst. Growth* **446**, 39 (2016).
- [22] J. Cieślak and S. M. Dubiel, *Nucl. Instrum. Methods B* **95**, 131 (1995).
- [23] P. Bonville, F. Rullier-Albenque, D. Colson, and A. Forget, *EPL* **89**, 67008 (2010).
- [24] J. Hesse and A. Rübartsch, *J. Phys. E: Sci. Instrum.* **7**, 526 (1974).
- [25] G. Le Caër and J. M. Dubois, *J. Phys. E: Sci. Instrum.* **12**, 1083 (1979).
- [26] S. M. Dubiel, *J. Alloys Compd.* **488**, 18 (2009).
- [27] Q. Huang, Y. Qiu, W. Bao, M. A. Green, J. W. Lynn, Y. C. Gasparovic, T. Wu, G. Wu, and X. H. Chen, *Phys. Rev. Lett.* **101**, 257003 (2008).
- [28] A. I. Goldman, D. N. Argyriou, B. Ouladdiaf, T. Chatterji, A. Kreyssig, S. Nandi, N. Ni, S. L. Bud'ko, P. C. Canfield, and R. J. McQueeney, *Phys. Rev. B* **78**, 100506(R) (2008).
- [29] J. Zhao, W. Ratcliff II, J. W. Lynn, G. F. Chen, J. L. Luo, N. L. Wang, J. Hu, and P. Dai, *Phys. Rev. B* **78**, 140504(R) (2008).
- [30] Y. Xiao, Y. Su, M. Meven, R. Mittal, C. M. N. Kumar, T. Chatterji, S. Price, J. Persson, N. Kumar, S. K. Dhar, A. Thamizhavel, and Th. Brueckel, *Phys. Rev. B* **80**, 174424 (2009).
- [31] J. G. Analytis, H.-H. Kuo, R. D. McDonald, M. Wartenbe, P. M. C. Rourke, N. E. Hussey, and I. R. Fisher, *Nature Phys.* **10**, 194 (2014).
- [32] U. D. Wdowik and K. Ruebenbauer, *Phys. Rev. B* **76**, 155118 (2007).
- [33] T. Goltz, V. Zinth, D. Johrendt, H. Rosner, G. Pascua, H. Luetkens, P. Materne, and H.-H. Klauss, *Phys. Rev. B* **89**, 144511 (2014).
- [34] I. Nowik, I. Felner, N. Ni, S. L. Bud'ko, and P. C. Canfield, *J. Phys.: Condens. Matter* **22**, 355701 (2010).
- [35] P. Wang, Z. M. Stadnik, J. Żukrowski, A. Thaler, S. L. Bud'ko, and P. C. Canfield, *Phys. Rev. B* **84**, 024509 (2011).
- [36] A. Khasanov, S. C. Bhargava, J. G. Stevens, J. Jiang, J. D. Weiss, E. E Hellstrom, and A. Nath, *J. Phys.: Condens. Matter* **23**, 202201 (2011).
- [37] S. Sharma, A. Bharathi, S. Chandra, V. R. Reddy, S. Paulraj, A. T. Satya, V. S. Sastry, A. Gupta, and C. S. Sundar, *Phys. Rev. B* **81**, 174512 (2010).
- [38] N. Ni, S. L. Bud'ko, A. Kreyssig, S. Nandi, G. E. Rustan, A. I. Goldman, S. Gupta, J. D. Corbett, A. Kracher, and P. C. Canfield, *Phys. Rev. B* **78**, 014507 (2008).

- [39] A. Błachowski, K. Ruebenbauer, J. Żukrowski, and Z. Bukowski, *J. Alloys Compd.* **582**, 167 (2014).
- [40] K. Komeđera, A. K. Jasek, A. Błachowski, K. Ruebenbauer, and A. Krztoń-Maziopa, *J. Magn. Magn. Mater.* **399**, 221 (2016).
- [41] G. Kresse and J. Furthmüller, VASP (University of Vienna, Austria, 1999); *Comput. Mater. Sci.* **6**, 15 (1996); G. Kresse and J. Hafner, *Phys. Rev. B* **47**, 558 (1993); G. Kresse and J. Furthmüller, *ibid.* **54**, 11169 (1996).
- [42] P. Blaha, K. Schwarz, G. K. H. Madsen, D. Kvasnicka, and J. Luitz, *Wien2k, An Augmented Plane Wave and Local Orbitals Program for Calculating Crystal Properties*, edited by K. Schwarz (Vienna University of Technology, Austria, 2001, ISBN 3-9501031-1-2).
- [43] P. E. Blöchl, *Phys. Rev. B* **50**, 17953 (1994); G. Kresse and D. Joubert, *ibid.* **59**, 1758 (1999); G. Kresse and J. Furthmüller, *Phys. Rev. B* **54**, 11169 (1996); G. Kresse and J. Furthmüller, *Comput. Mater. Sci.* **6**, 15 (1996).
- [44] J. P. Perdew, K. Burke, and M. Ernzerhof, *Phys. Rev. Lett.* **77**, 3865 (1996); **78**, 1396 (1997); J. P. Perdew, A. Ruzsinszky, G. I. Csonka, O. A. Vydrov, G. E. Scuseria, L. A. Constantin, X. Zhou, and K. Burke, *Phys. Rev. Lett.* **100**, 136406 (2008).
- [45] A. Mewis, *Z. Naturforsch. B: J. Chem. Sci.* **35**, 141 (1980).
- [46] U. D. Wdowik, *Phys. Rev. B* **84**, 064111 (2011); A. Błachowski, U. D. Wdowik, and K. Ruebenbauer, *J. Alloy Compd* **486**, 36 (2009).
- [47] R. Bader, *Atoms in Molecules: A quantum Theory* (Oxford University Press, New York, 1990).

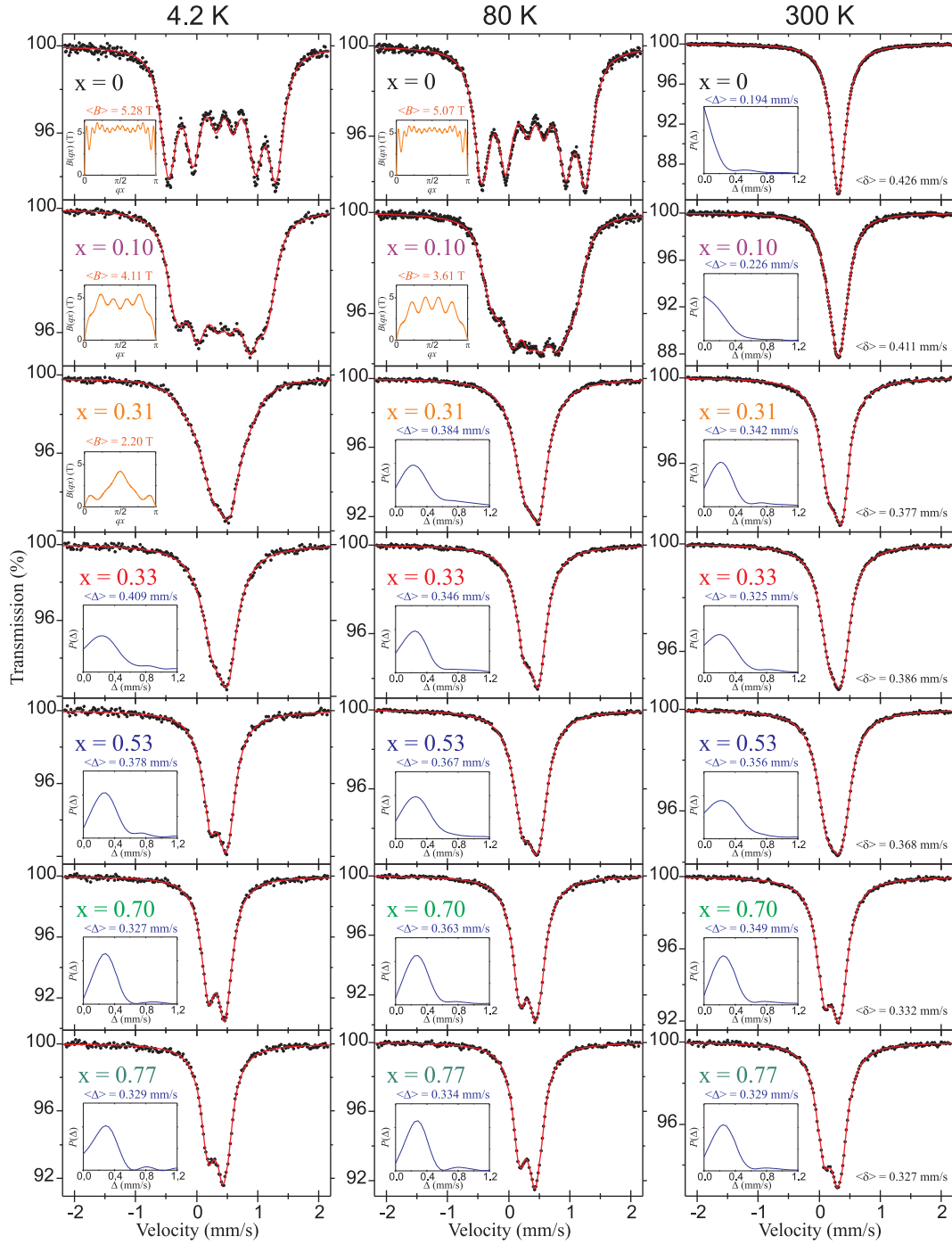


Fig.1 ^{57}Fe Mössbauer spectra of $\text{BaFe}_2(\text{As}_{1-x}\text{P}_x)_2$ measured at 4.2 K, 80 K and 300 K. (Insets) Shapes of the SDW with the average magnetic hyperfine field $\langle B \rangle$ and normalized distributions of the electric quadrupole splitting with the average value $\langle \Delta \rangle$. The average center shifts $\langle \delta \rangle$ of spectra measured at 300 K are shown.

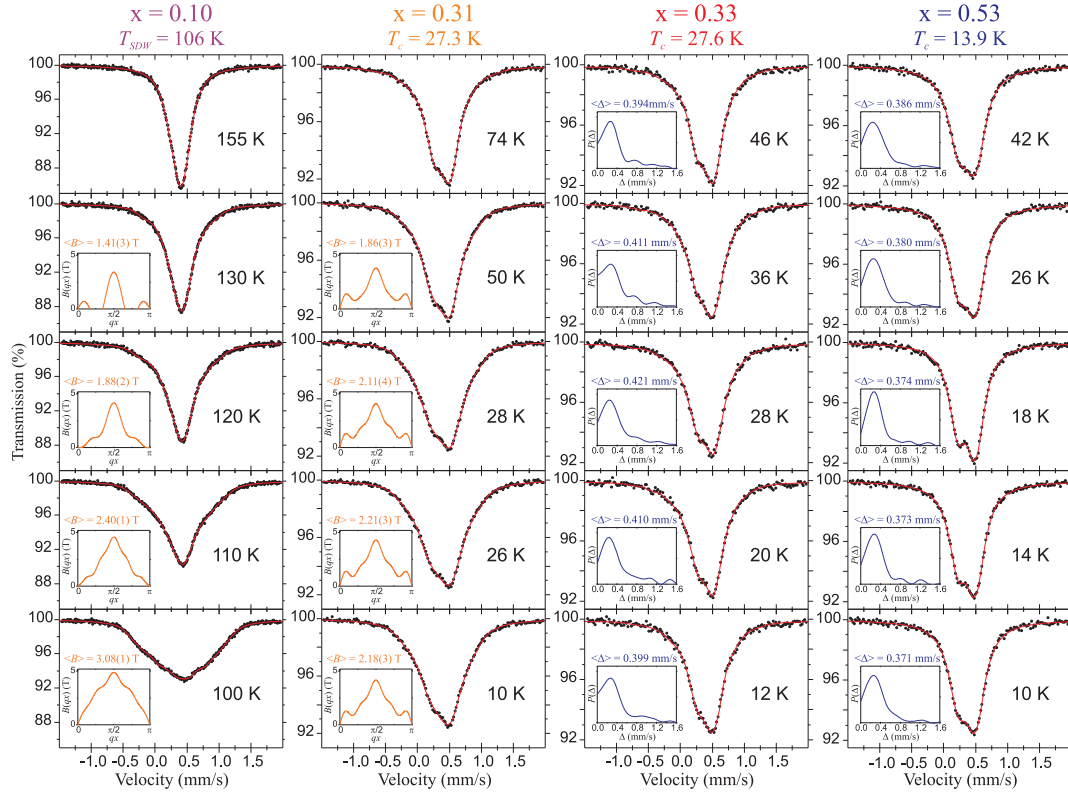


Fig. 2 Selected ^{57}Fe Mössbauer spectra of $\text{BaFe}_2(\text{As}_{1-x}\text{P}_x)_2$ versus temperature across the nematic phase region (for $x = 0.10$) and across transition to the superconducting state (for $x = 0.31, 0.33,$ and 0.53). Spectra measured for particular compounds at the same conditions during non-interrupted series are shown for comparison on the same scale. (Insets) Shapes of the SDW with the average magnetic hyperfine field $\langle B \rangle$ and the distributions of the electric quadrupole splitting with the average value $\langle \Delta \rangle$. For nematic region the SDW shapes should be interpreted as the incoherent spin density wavelets. The temperature of the coherent SDW magnetic order T_{SDW} and the critical temperatures of superconducting transitions T_c are indicated in the headline.

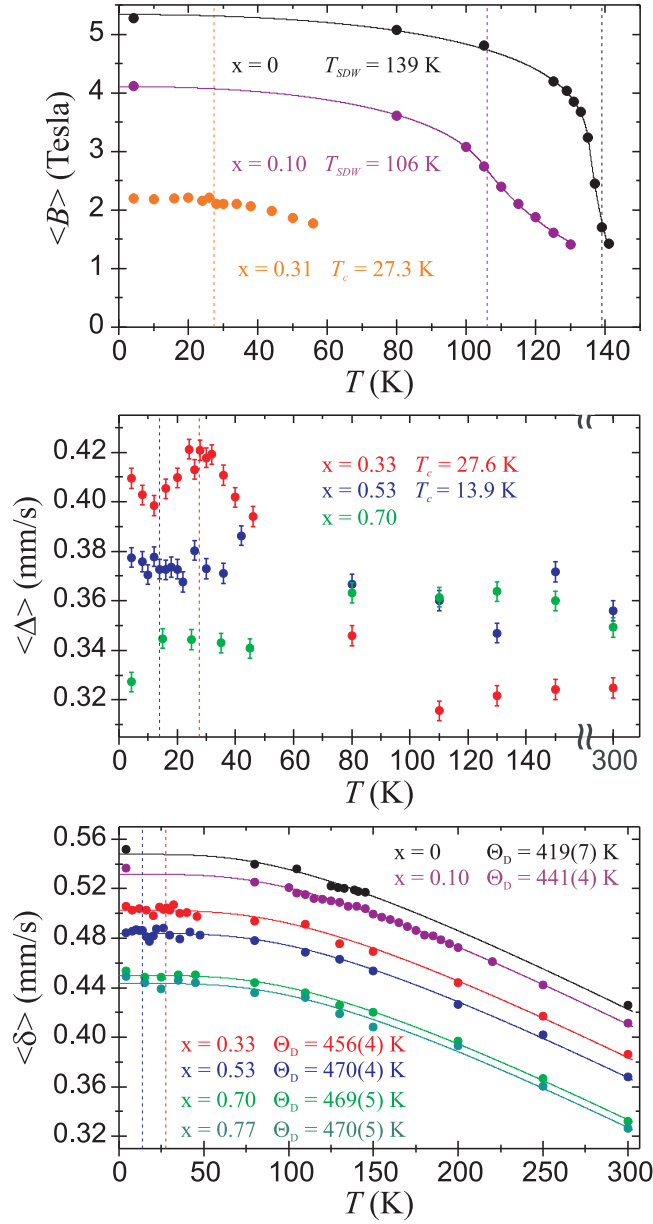


Fig. 3 Temperature dependencies of the Mössbauer spectroscopy parameters: the average magnetic hyperfine field of the SDW $\langle B \rangle$, the average electric quadrupole splitting $\langle \Delta \rangle$, and the average spectral center shift $\langle \delta \rangle$. The coherent SDW magnetic order temperatures T_{SDW} , the critical temperatures of superconducting transitions T_c , and the Debye temperatures Θ_D are shown for $\text{BaFe}_2(\text{As}_{1-x}\text{P}_x)_2$ compounds with different phosphorus substitution level x . Vertical dashed lines mark the respective temperatures T_{SDW} and T_c . The solid lines represent the best-fit to the experimental data, using the Debye model for $\langle \delta \rangle(T)$ and the model described in Ref. [16] for $\langle B \rangle(T)$. Typical errors for $\langle B \rangle$ and $\langle \delta \rangle$ are 0.03 T and 0.003 mm/s, respectively.

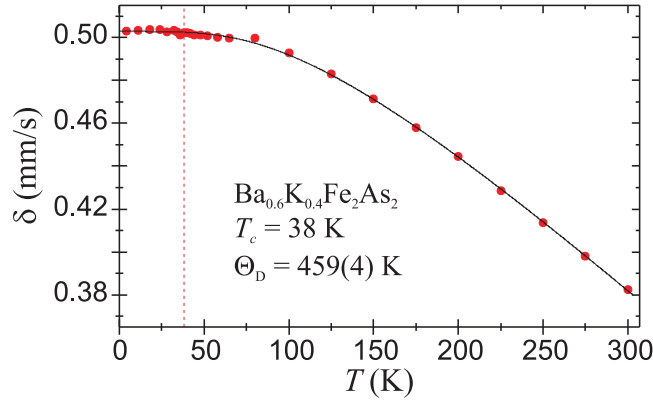


Fig. 4 The Mössbauer spectra center shift δ versus temperature for optimally hole-doped superconductor $\text{Ba}_{0.6}\text{K}_{0.4}\text{Fe}_2\text{As}_2$. Experimental data are taken from Ref. [18] and partly unpublished results. Vertical dashed line marks the critical temperature $T_c = 38$ K. The solid line represents the best-fit to the experimental data according to the Debye model with the resulting Debye temperature $\Theta_D = 459$ K.

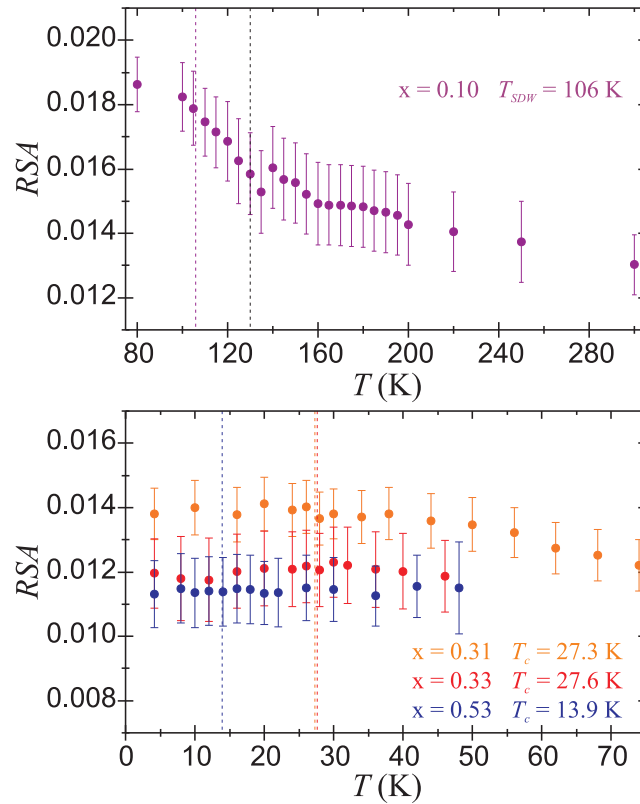


Fig. 5 Temperature dependencies of the relative spectral area (RSA) for $\text{BaFe}_2(\text{As}_{1-x}\text{P}_x)_2$ (under-doped and superconductors). Vertical dashed lines mark T_{SDW} and T_c temperatures. The nematic order temperature [7] for $x = 0.10$ is denoted by black dashed line at 130 K. Each RSA is derived from series of measurements performed at constant conditions (see text for details). Note: despite identical weights of samples the sets of RSA may not be comparable between each other due to possible differences in the resonant thicknesses between particular absorbers.

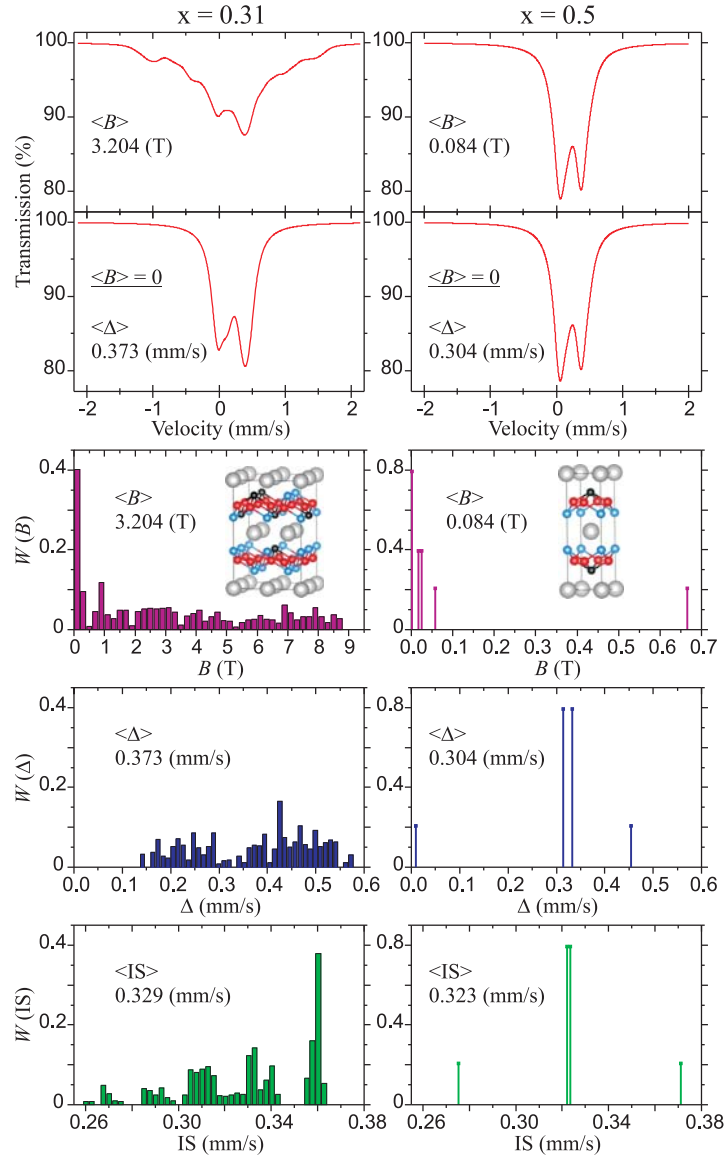


Fig. 6 Simulated ^{57}Fe Mössbauer spectra for $\text{BaFe}_2(\text{As}_{1-x}\text{P}_x)_2$ with $x = 0.31$ and $x = 0.5$, and calculated distributions of the magnetic hyperfine field B , the electric quadrupole splitting Δ , and the chemical isomer shift IS versus $\alpha\text{-Fe}$ (with δ_{SOD} neglected). The numbers indicate respective average values. (Insets) Schematic examples of the simulated configurations with gray, red, blue, and black balls denoting Ba, Fe, As, and P atoms, respectively.